Journal of Renewable Materials

Tech Science Press

DOI: 10.32604/jrm.2021.015189

ARTICLE

Recycling of Mud Derived from Backwash Wastewater Coagulation as Magnetic Sodalite Sphere for Zn^{2+} Adsorption

Suiyi Zhu[1], Manhong Ji[1], Hongbin Yu[1,*], Zhan Qu[1], Jiakuan Yang[2], Mingxin Huo[1] and Yi Wang[1]

[1]School of Environment, Northeast Normal University, Changchun, 130024, China

[2]School of Environmental Science & Engineering, Huazhong University of Science and Technology, Wuhan, 430074, China

[*]Corresponding Author: Hongbin Yu. Email: papermanuscript@126.com

Received: 29 November 2020 Accepted: 29 January 2021

ABSTRACT

Herein, we reported a method to prepare magnetic sodalite sphere by using the mud from backwash wastewater after polyaluminum chloride (PAC) coagulation. The results showed that approximately 100% of Fe in the wastewater was precipitated as flocculent iron mud (FM) by adding PAC. FM was converted to spherical magnetic sodalite (FMP) with a diameter of 3 μm via a facile alkali hydrothermal method without adding Al/Si resources or reductant. The product FMP had the saturated magnetization of 10.9 emu g^{-1} and high Zn^{2+} adsorption capacity of 50.6 mg g^{-1}. Without coagulation with PAC, the removal rate of Fe from the wastewater was only 92.7%, and the precipitated mud (RM) was converted to irregular particles (RMP), which had weak magnetic response and low capacity of Zn^{2+} adsorption comparing with FMP. With the method, the Fe in backwash wastewater was effectively recycled, and the generated sludge was converted to well-formed sodalite sphere without generating any secondary waste.

KEYWORDS

Backwash wastewater; coagulation; magnetic sodalite; Mössbauer; adsorption

1 Introduction

Backwash wastewater was commonly generated from sand filtration process in groundwater plant, which was brownish suspension and contained high concentration of free Fe and suspended Si/Al particles [1,2]. The wastewater accounted for 3%–5% of the produced water in groundwater plant [3]. In many countries and regions, such wastewater was recharged directly into well or discharged into river and/or lake, where free Fe was released and potentially polluted the water nearby [4]. With the regulation of environmental management, such wastewater should be properly treated before discharge. When the wastewater was placed stand for several days, the suspended particles, along with the hydrolysed flocs of Fe, were spontaneously precipitated as brownish mud [5]. Such mud was generally treated by mechanical filtration and solidified before sending to landfill [6]. Thereby, the disposal of backwash wastewater was tedious and entails extra cost.

The mud generated from backwash wastewater, is rich in Si/Al oxides and FeOOH, which have effective coordination sites, including $Si–O^-$, $Al–O^-$, and $Fe–O^-$ [7], for adsorption of cations, such as Zn^{2+}, Cd^{2+}, Ni^{2+} [8], and negative ions, such as phosphate [9], from wastewater. However, after use, tedious

This work is licensed under a Creative Commons Attribution 4.0 International License, which permits unrestricted use, distribution, and reproduction in any medium, provided the original work is properly cited.

separation of the mud from wastewater were performed, including centrifugation and/or filtration [10]. To avoid the tedious treatment, the mud can be converted into magnetic particles via thermal treatment [11] and/or calcination [12]. For instance, Zhu et al. [11] hydrothermally treated a FeOOH-bearing mud at 160°C for 10 h, and found that magnetite-bearing product were generated in the presence of reductants, e.g., ethylene glycol or ascorbic acid. Without the reductant, such weakly crystallized FeOOH in the mud was converted to maghemite and hematite [13]. But the conversion was slow because the impure Si and Al occupied the surface site of FeOOH, and then inhibited the conjunction of surface hydroxyl groups as Fe-O-Fe bond [13,14]. Thereby, the corresponding product exhibited a weak magnetic response. The Si/Al oxides in mud can be dissolved under highly alkaline condition [15]. Thus, the transformation of FeOOH to maghemite and hematite maybe accelerated, which employed an acceptable route to recycle Fe/Si/Al-bearing mud.

Recently, to recycle backwash wastewater, it was pre-treated with coagulation and precipitation, and then purified with a combined sand filter and ultrafiltration route [16,17]. This process provided extra Al and then complicated the mud composition. Up to date, only a few reports concerned the upcycling of Fe/Al/Si-bearing waste as magnetic material.

In this study, the object was to investigate the recycling of coagulated sludge from backwash wastewater, as magnetic sodalite sphere. The addition of PAC in the coagulation of backwash wastewater had two apparent merits, one of which was to removal Fe from wastewater at a high level, and the other was to introduce exogenous Al in the involvement of sodalite formation. The formation mechanism for magnetic species and sodalite was analyzed and the application of magnetic sodalite sphere in Zn-bearing wastewater was also investigated.

2 Materials and Methods

2.1 Backwash Wastewater Pre-Treatment

Backwash wastewater with initial Fe concentration of 87.5 mg L^{-1} was acquired from the reservoir of Kulunqi water supply (Inner Mongolia, China). It was treated as follows. 0.5 g PAC was dispersed in 25 L of backwash wastewater under vigorously agitating at 50 rpm for 10 min. After sedimentation for 30 min, the precipitated iron mud (named as FM) was collected and vacuum-dried at 50°C overnight. In control experiment, the backwash wastewater was placed on the table without stirring in the absence of PAC, and the generated mud was named as RM.

2.2 The Process of MS Synthesis

FM and RM were recycled in the following steps. 0.6 g of FM was added to 30 mL of 1.5 M NaOH and mixed at 200 rpm for 10 min. The generated suspension was transferred to a 50 mL Teflon vessel and autoclaved at 160°C for 10 h. After that, a blackish precipitate was generated at the vessel bottom, and collected with a magnet, followed by washing 5 times with deionized water and vacuum-dried overnight. Same procedure was performed on the treatment of RM. The synthesized magnetic particles from FM and RM were named as FMP and RMP, respectively.

2.3 Application in Zn-Bearing Wastewater Treatment

The adsorption experiment was carried out as follows. For FMP, 20 mL of $ZnSO_4$ with desired concentrations was mixed with 0.02 g of FMP in a 50 mL Erlenmeyer flask sealed with parafilm. The flask was shaken at 150 rpm at 30°C for 24 h in an incubator shaker (THZ-98A, Yiheng, China). After that, the used FMP was separated from the supernatant by attaching a magnet to the flask. Zn^{2+} in the supernatant was analysed by using an inductively coupled plasma optical emission spectrometry (ICP-OES, AVIO-200, PerkinElmer, USA). Similar experiment of Zn^{2+} adsorption was carried out using RMP as adsorbent. The capacities of FMP and RMP adsorption (q_e, mg g^{-1}) were calculated by using Eq. (1).

$$q_e = \frac{(C_0 - C_e) \times V}{m} \quad (1)$$

where, C_0 is the initial concentration (mg L^{-1}); C_e is the equilibrium concentration (mg L^{-1}); V is the volume of the solution (L); m is the mass of FMP/RMP (g).

The adsorption experiments in this study were performed in triplicate, and the average of the values was reported. The experimental data were subjected to one-way analysis of variance using Microsoft Excel (v. 2016, Microsoft, USA), and the differences between the sets of data were not statistically significant.

2.4 Characterization of the Sludges and Products

The X-ray diffraction (XRD) patterns of the sludges, RMP and FMP, were determined by diffractometry (RAPID-S; Rigaku, Japan) with Cu-Kα radiation in the 2θ range of 10°–70°. Transmission Mössbauer spectroscopy experiments were performed using a spectrometer (MP500; Oxford, UK) at room temperature. The data of saturation magnetization was detected at room temperature by magnetometry (Quantum Design, USA) with a SQUID-VSM system. The morphology was analyzed by field-emission scanning electron microscopy (SEM, FEI Co., USA). The composition of the sludges, RMP and FMP, was determined by X-ray fluorescence (ARL Advant XP^+; Thermo, USA).

3 Results and Discussion

3.1 Fe Removal from Backwash Wastewater

Backwash wastewater was treated by coagulation with PAC, and the removal rate of Fe from the backwash wastewater was nearly 100%. This amount was apparently higher than that without adding PAC (92.7%). When PAC was dispersed into the backwash wastewater for facilitating settlement of particles, many polymeric species were generated with its hydrolysis, such as $Al_6(OH)_{15}^{3+}$, $Al_{13}O_4(OH)_{24}^{7+}$ and $Al_{13}(OH)_{34}^{5+}$ [18]. The newly formed Al species were active in adsorption of the Fe-containing colloids in backwash wastewater via surface complexation [19,20] and trapping of the Fe/Si oxides microparticles [21], and polymerized in the form of $Al(OH)_3$ flocks. These flocks were precipitated rapidly in comparison with the Fe-containing colloids (Fig. 1), resulting in a clarified backwash wastewater.

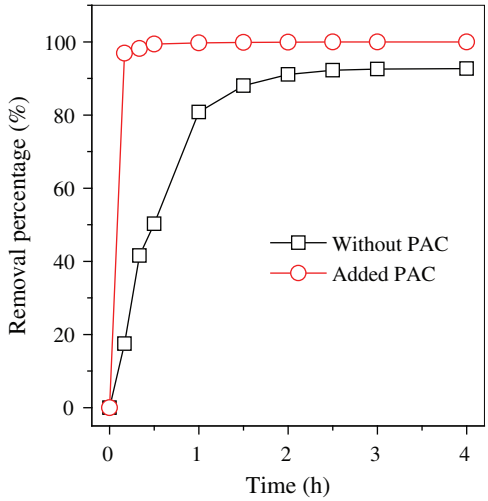

Figure 1: Fe removal from backwash wastewater with and without adding PAC

3.2 Formation of Magnetic Maghemite

The two muds, RM and FM, had high Fe content and numerous impurities of Si/Al oxides (Tab. 1). The Fe-bearing compounds were identified by Mossbauer spectroscopy (Fig. 2 and Tab. 2), and the results showed that 2-line ferrihydrite was predominant in RM and FM. When the two muds were treated by hydrothermal method, the phase transformation of 2-line ferrihydrite occurred. The diffraction peaks of X-ray diffraction (XRD) were located at $2\theta = 33.1°$ and 35.7° (Fig. 3a), which attributed to hematite and maghemite, respectively, and became intensified after the hydrothermal treatment. This finding suggested the conversion of ferrihydrite to maghemite and hematite. The directly conversion of ferrihydrite to hematite was initially fast under aerobic condition [14], but slow down with the accumulation of impurities, such as Al [14] and Si [15], where intermediate maghemite was generated. The corresponding area of maghemite in Mössbauer subspectrum demonstrated that it accounted for 14.2% of the total Fe in RMP (Fig. 2 and Tab. 2), lower than that (18.3%) in FMP.

Table 1: Chemical composition of RM, RMP, FM, and FMP

Composition (wt.%)	RM	RMP	FM	FMP
Fe_2O_3	48.15	68.41	33.11	62.61
SiO_2	8.81	8.86	7.96	14.57
Al_2O_3	2.08	1.64	14.18	11.73
Na_2O	0.049	2.47	0.0286	5.94
MnO	6.18	9.39	0.858	1.72
P_2O_5	3.48	1.92	2.44	0.78
CaO	2.79	4.87	0.616	1.28
Si/Al mole ratio	3.6	4.59	0.48	1.06

Maghemite was a well-known magnetic specie. The presence of maghemite in RMP/FMP products showed that they had good magnetic response and was easily separated from water. As shown in Fig. 3b, both RM and FM demonstrated weak magnetic responses due to the absence of maghemite, but became stronger with the conversion of ferrihydrite to maghemite after hydrothermal treatment. However, the product FMP, synthesized with FM, had high content of maghemite (Tab. 2), and exhibited superior saturated magnetization of 10.9 emu g^{-1}, comparing with them of RMP, due to the high content of maghemite in FMP comparing with that in RMP.

3.3 Formation of Sodalite Sphere

The muds and corresponding products were characterized by SEM. Fig. 4a showed that RM was in the form of irregular aggregates. After hydrothermal treatment, no obvious change in morphology was observed (Fig. 4b). After the treatment of backwash wastewater with PAC, the generated FM showed a similar amorphous morphology to RM (Fig. 4c). However, FMP prepared using FM as raw material, demonstrated a large quantity of spherical particles with an average diameter of 3 μm (Fig. 4d).

The phase transformation of Si/Al oxides was investigated by XRD method. As shown in Fig. 3a, FM showed the peaks of quartz and boehmite, which disappeared after hydrothermal treatment. Instead, new diffraction peaks occurred at $2\theta = 14°$, 24.5°, 35°, and 43.2°, which can be attributed to the sodalite phase (JCPDS 31-1271) from quartz and boehmite recrystallization [22]. When RM was treated by the hydrothermal method, the peaks of quartz disappeared due to the dissolution of quartz under alkaline

condition [4,23], but no peaks of sodalite was observed, indicating that the sodalite was not formed in RMP due to the lack of Al source. The Si/Al ratio was important for sodalite synthesis. Tab. 1 shows that the Si/Al ratio in FM was 0.48. This value was smaller than that in RM (3.6). The low Si/Al ratio was attributed to the PAC added in the flocculation of backwash wastewater. After hydrothermal treatment, the Si/Al ratio increased to 1.06, approximated to the Si/Al ratio in sodalite [22]. In addition, the Na content of FMP was higher than that in RMP due to the sodalite formation (Tab. 1). The high Na in FMP was caused by captured Na ions to neutralize the minus charge on aluminate or silicate in sodalite structure when sodalite crystal was formed [24].

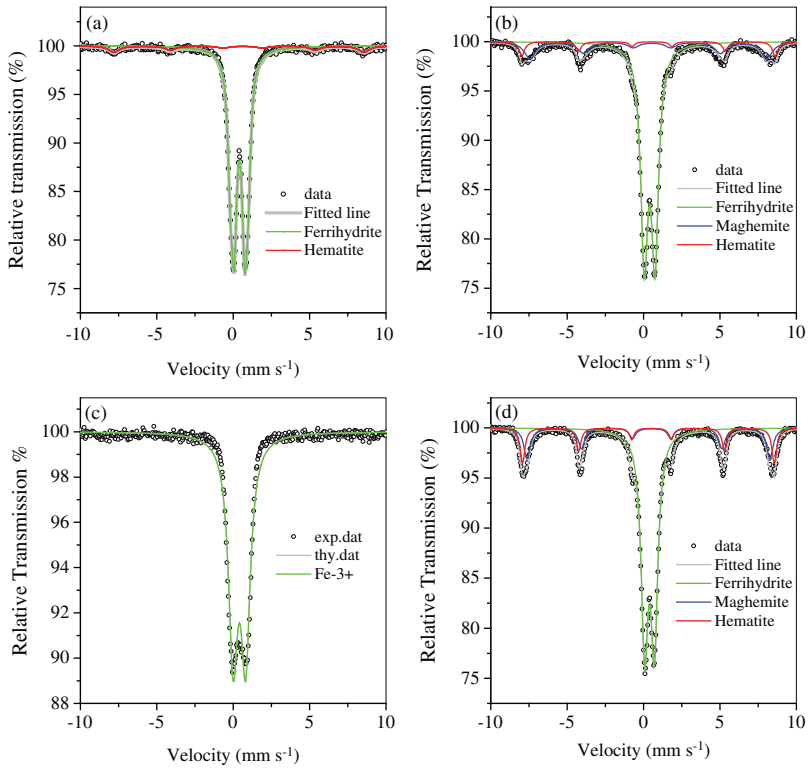

Figure 2: Mössbauer spectrum of RM (a), RMP (b), FM (c) and FMP (d)

Table 2: Mössbauer parameters of RM, RMP, FM and FMP

Sample	Component	*IS*[a] (mm s^{-1})	*QS*[b] (mm s^{-1})	H_{in}[c] (KOe)	Ratio[d] (%)
RM	Ferrihydrite	0.26	0.71		91.2
	Hematite	0.28	0.21	510.8	8.8
RMP	Ferrihydrite	0.26	0.7		73.1
	Maghemite	0.3	0.24	480.4	14.2
	Hematite	0.3	0.23	513.5	12.7
FM	Ferrihydrite	0.26	0.82		100
FMP	Ferrihydrite	0.25	0.63		66.2
	Maghemite	0.29	0.21	492.7	18.3
	Hematite	0.28	0.21	510.8	15.5

Note: [a] *IS*, isomer shift, related to α-Fe; [b] *QS*, electric quadrupole splitting; [c] H_{in}, Hyperfine field; [d] Ratio, spectral area ratio.

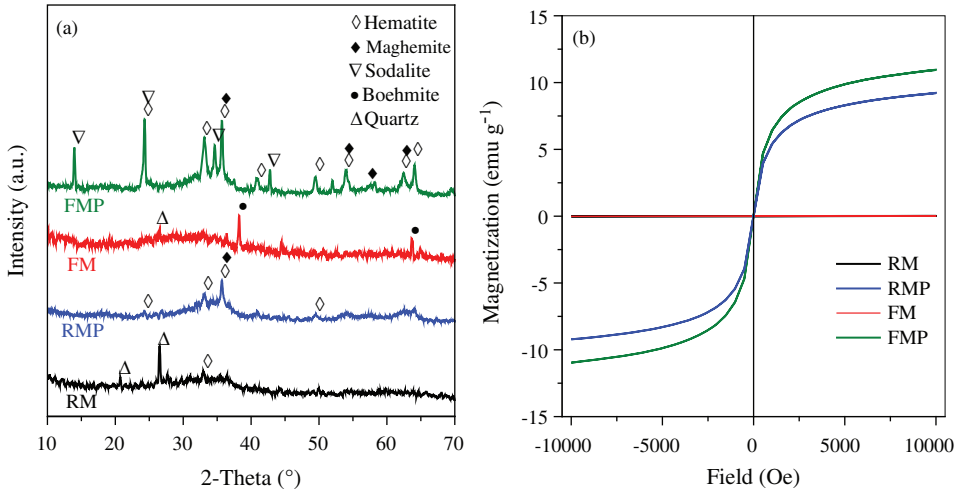

Figure 3: (a) XRD patterns and (b) room-temperature magnetization curves of RM, RMP, FM, and FMP

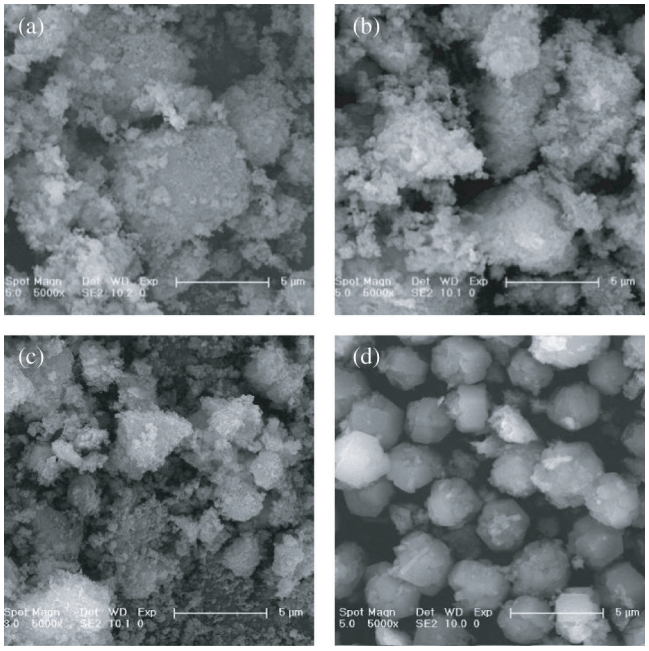

Figure 4: SEM pictures of RM (a), RMP (b), FM (c) and FMP (d)

3.4 Formation Mechanism of Magnetic Sodalite

In the backwash wastewater, Fe was in three species, e.g., Fe-bearing flocs, colloids, and free Fe ions. A portion of Fe species were coordinated on the surface of broken quartz filter and sand, and naturally precipitated to the bottom of backwash wastewater. Other Fe-bearing colloids and flocs, were fine particles, which were suspended and did not precipitate even though the backwash wastewater was kept stand for a long time. For instance, approximately 6.4 mg/L Fe was residual after the wastewater was precipitated for 4 h. With the addition of polymeric aluminium chloride (PAC), it was hydrolysed to Al-bearing oxyhydroxide with plenty of hydroxyl groups for free Fe coordination, and then promoted the polymerization of Fe-bearing colloid via bridging effect, resulting in the removal of Fe from backwash wastewater at high level. With the Fe removal, Al was involved in the precipitates in the wastewater treatment.

In the sludges, such Fe species were in the weakly crystallized form (commonly as Ferrihydrite), and coordinated on the Al/Si minerals surface. With hydrothermal treatment, the phase transformation of Ferrihydrite and the dissolution-recrystallization of Si/Al impurities occurred, with the formation of magnetic sodalite. This process included four steps. First, Si/Al impurities, e.g., quartz and boehmite, were dissolved in NaOH solution, to generate and release of SiO_3^{2-} and $Al(OH)_4^-$ to liquid solution. Second, the conjunction reaction of two adjacent hydroxyl groups on each Ferrihydrite particles occurred, to release of one water molecule, with the generation of Fe–O–Fe bond. As the conjunction reaction continued, hematite was generated, with maghemite being intermediate. It has been reported that pure ferrihydrite was rapidly transformed into hematite [25]. But, in the presence of impurities, such as Si and Al, they occupied the surface sites of Ferrihydrite, and accordingly inhibited the conjunction of adjacent Ferrihydrite, and the following regular array of Fe–O–Fe bond, with maghemite as final product [25,26]. Third, when the dissolved SiO_3^{2-} and $Al(OH)_4^-$ were supersaturated, the crystallization of Si/Al oxides occurred on the crystallized Fe oxides surface. Forth, as the recrystallization of Si/Al impurities continued, an Si/Al cover were generated and then involved in the spherical sodalite formation.

However, without adding PAC, the generated sludge, RM, was poor in Al and rich in Si, so that only the dissolution of Si occurred in alkaline solution. When the Si concentration became saturated, e.g., at approximately 6000 mg/L, the dissolution of impure Si did not continue, led to the residue Si on the surface sites of Ferrihydrite. This apparently inhibited the transformation of Ferrihydrite to hematite and maghemite. Different with RM, FM comprised of Al/Si after PAC coagulation, and accordingly the simultaneous dissolution-recrystallization of Si/Al took placed, with the residue of Si/Al were less than 700 mg/L. This process accelerated the continuous dissolution of impure Si/Al, and the phase transformation of Ferrihydrite to hematite and maghemite. Thereby, the magnetic sodalite, FMP, showed a high magnetization in comparison with RMP.

3.5 Adsorption Performance of Magnetic Sodalite Sphere

The adsorption performance of RMP and FMP were investigated by using Zn^{2+} as the potential pollutant. Higher capacity of Zn^{2+} adsorption was observed by FMP than RMP (Fig. 5a), probably because of the high content of Na^+ induced in the recrystallization of sodalite in FMP. Na^+ on the active sites of sodalite, such as $\equiv$Si–O$^-$ and $\equiv$Al–O$^-$ [27], can be replaced by Zn^{2+} via cationic exchange reaction [4]. The adsorption of Zn^{2+} by FMP and RMP fitted well with the Langmuir isotherm model (Fig. 5b), indicating that the two particles had energy-balanced surface and the adsorption of Zn was belonged to the monolayer adsorption. The maximum capacity of Zn^{2+} adsorption was 50.6 mg g^{-1} by FMP, which was remarkablly higher than 24.3 mg g^{-1} of RMP, and other synthesized adsorbents from iron mud, such as 19.8 mg g^{-1} of magnetic nanoplatelet particles [4] and 14.9 mg g^{-1} of CO_2-neutralized red mud [28], indicating that FMP had great potential in Zn^{2+} adsorption.

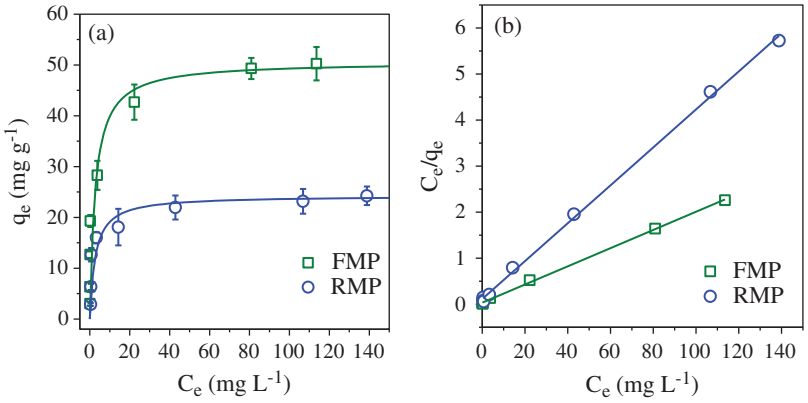

Figure 5: (a) Zn^{2+} adsorption on PMP and FMP; (b) Conversion of Langmuir isotherm model to the linear fitting plots to determine its parameters of C_e and q_e

4 Conclusion

Backwash wastewater was effectively treated with the addition of PAC, and accordingly the generated sludge was a mixture of ferrihydrite, quartz, boehmite and other impurities. After hydrothermal treatment with the addition of NaOH, the sludge was converted into magnetic sodalite sphere. The conversion took placed in the following steps, (1) the dissolution of impurities quartz and boehmite, (2) the phase transformation of ferrihydrite to maghemite and hematite, (3) the recrystallization of Al/Si on the surface of Fe-bearing species, and (4) the crystal growth of Al/Si to sodalite sphere. In the absence of PAC, the precipitated sludge from backwash wastewater was converted into irregular magnetic aggregates, and showed a weak magnetization and a low adsorption capacity of Zn^{2+} in comparison with that with PAC.

Availability of Data and Materials: All data generated or analyzed during this study are included in this published article.

Funding Statement: This work was supported by the National Key Research and Development Program of China (Grant No. 2019YFE0117900), the National Natural Science Foundation of China (Grant Nos. 52070038 and 51878134) and the Science and Technology Program of Jilin Province (Grant No. 20190303001SF).

Conflicts of Interest: The authors declare that they have no conflicts of interest to report regarding the present study.

References

1. Dotremont, C., Molenberghs, B., Doyen, W., Bielen, P., Huysman, K. (1999). The recovery of backwash water from sand filters by ultrafiltration. *Desalination, 126(1–3),* 87–94. DOI 10.1016/S0011-9164(99)00158-7.
2. Katsoyiannis, I. A., Zouboulis, A. I. (2004). Biological treatment of Mn(II) and Fe(II) containing groundwater: Kinetic considerations and product characterization. *Water Research, 38(7),* 1922–1932. DOI 10.1016/j.watres.2004.01.014.
3. Wiercik, P., Matras, K., Burszta-Adamiak, E., Kuśnierz, M. (2016). Analysis of the properties and particle size distribution of spent filter backwash water from groundwater treatment at various stages of filters washing. *Engineering and Protection of Environment, 19(1),* 149–161. DOI 10.17512/ios.2016.1.12.
4. Zhu, S., Dong, G., Yu, Y., Yang, J., Yang, W. et al. (2018). Hydrothermal synthesis of a magnetic adsorbent from wasted iron mud for effective removal of heavy metals from smelting wastewater. *Environmental Science and Pollution Research International, 25(23),* 22710–22724. DOI 10.1007/s11356-018-2378-3.
5. Zimoch, I., Lasocka-Gomua, I. (2015). Potential operational effectiveness of backwash water recirculation in groundwater treatment train of mosina plant near Poznan. *Ochrona Środowiska, 37(3),* 49–55.
6. Zhao, Y., Chen, P., Wang, S., Ji, Y., Wang, Y. et al. (2020). Utilization of bayer red mud derived from bauxite for Belite-Ferroaluminate cement production. *Journal of Renewable Materials, 8(11),* 1531–1541. DOI 10.32604/jrm.2020.011462.
7. Ong, D. C., Kan, C. C., Pingul-Ong, S. M. B., Luna, M. D. G. D. (2017). Utilization of groundwater treatment plant (GWTP) sludge for nickel removal from aqueous solutions: Isotherm and kinetic studies. *Journal of Environmental Chemical Engineering, 5(6),* 5746–5753. DOI 10.1016/j.jece.2017.10.046.
8. Jaafar, A. R., Isa, M. H., Kutty, S. R. M. (2008). Adsorption of zinc, cadmium and nickel from aqueous solutions using ground water sludge (GWS). *WIT Transactions on Ecology and the Environment, I,* 247–253. DOI 10.2495/WP080241.
9. Bal Krishna, K. C., Aryal, A., Jansen, T. (2016). Comparative study of ground water treatment plants sludges to remove phosphorous from wastewater. *Journal of Environmental Management, 180(10),* 17–23. DOI 10.1016/j.jenvman.2016.05.006.
10. Zhu, S., Lin, X., Dong, G., Yu, Y., Yu, H. et al. (2019). Valorization of manganese-containing groundwater treatment sludge by preparing magnetic adsorbent for Cu(II) adsorption. *Journal of Environmental Management, 236,* 446–454. DOI 10.1016/j.jenvman.2019.01.117.

11. Zhu, S., Fang, S., Huo, M., Yu, Y., Chen, Y. et al. (2015). A novel conversion of the groundwater treatment sludge to magnetic particles for the adsorption of methylene blue. *Journal of Hazardous Materials, 292,* 173–179. DOI 10.1016/j.jhazmat.2015.03.028.
12. Hellgardt, K., Chadwick, D. (1999). Transformations of ferrihydrite during calcination and sulphidation. *Catalysis Today, 49(1–3),* 79–86. DOI 10.1016/S0920-5861(98)00411-8.
13. Zhu, S., Wu, Y., Qu, Z., Zhang, L., Yu, Y. et al. (2020). Green synthesis of magnetic sodalite sphere by using groundwater treatment sludge for tetracycline adsorption. *Journal of Cleaner Production, 247(1),* 119140. DOI 10.1016/j.jclepro.2019.119140.
14. Barrón, V., Torrent, J., Grave, E. D. (2003). Hydromaghemite, an intermediate in the hydrothermal transformation of 2-line ferrihydrite into hematite. *American Mineralogist, 88(11–12),* 1679–1688. DOI 10.2138/am-2003-11-1207.
15. Cornell, R. M. (1987). Effect of silicate species on the transformation of ferrihydrite into Goethite and Hematite in alkaline media. *Clays and Clay Minerals, 35(1),* 21–28. DOI 10.1346/CCMN.1987.0350103.
16. Dotremont, C., Molenberghs, B., Doyen, W., Bielen, P., Huysman, K. (1999). The recovery of backwash water from sand filters by ultrafiltration. *Desalination, 126(1–3),* 87–94. DOI 10.1016/S0011-9164(99)00158-7.
17. Zhang, H., Sun, M., Song, L., Guo, J., Zhang, L. (2019). Fate of NaClO and membrane foulants during *in-situ* cleaning of membrane bioreactors: Combined effect on thermodynamic properties of sludge. *Biochemical Engineering Journal, 147(6),* 146–152. DOI 10.1016/j.bej.2019.04.016.
18. Hu, C., Liu, H., Qu, J., Wang, D., Ru, J. (2006). Coagulation behavior of aluminum salts in eutrophic water: Significance of Al_{13} species and pH control. *Environmental Science & Technology, 40(1),* 325–331. DOI 10.1021/es051423+.
19. Ghosh, D., Solanki, H., Purkait, M. K. (2008). Removal of Fe(II) from tap water by electrocoagulation technique. *Journal of Hazardous Materials, 155(1−2),* 135–143. DOI 10.1016/j.jhazmat.2007.11.042.
20. Ellis, D., Bouchard, C., Lantagne, G. (2000). Removal of iron and manganese from groundwater by oxidation and microfiltration. *Desalination, 130(3),* 255–264. DOI 10.1016/S0011-9164(00)00090-4.
21. Chaturvedi, S., Dave, P. N. (2012). Removal of iron for safe drinking water. *Desalination, 303(3–4),* 1–11. DOI 10.1016/j.desal.2012.07.003.
22. Hu, T., Qiu, J., Wang, Y., Wang, C., Liu, R. et al. (2015). Synthesis of low Si/Al ratio hydroxysodalite from oil shale ash without pretreatment. *Journal of Chemical Technology & Biotechnology, 90(1),* 208–212. DOI 10.1002/jctb.4350.
23. Sun, M., Yan, L., Zhang, L., Song, L., Guo, J. et al. (2019). New insights into the rapid formation of initial membrane fouling after *in-situ* cleaning in a membrane bioreactor. *Process Biochemistry, 78(3),* 108–113. DOI 10.1016/j.procbio.2019.01.004.
24. Criado, M., Fernández-Jiménez, A., Palomo, A., Sobrados, I., Sanz, J. (2008). Effect of the SiO_2/Na_2O ratio on the alkali activation of fly ash. Part II: 29Si MAS-NMR Survey. *Microporous and Mesoporous Materials, 109(1−3),* 525–534. DOI 10.1016/j.micromeso.2007.05.062.
25. Barrón, V., Torrent, J., Grave, E. D. (2003). Hydromaghemite, an intermediate in the hydrothermal transformation of 2-line ferrihydrite into hematite. *American Mineralogist, 88(11−12),* 1679–1688. DOI 10.2138/am-2003-11-1207.
26. Barrón, V., Michel, F. M., Liu, Q., Koch, C. B., Torrent, J. (2012). Effects of Al(III) on the ferrihydrite-ordered ferrimagnetic ferrihydrite–hematite transformation. *European Geosciences Union General Assembly Conference,* Vienna, Austria.
27. Zhu, J., Pigna, M., Cozzolino, V., Caporale, A. G., Violante, A. (2013). Higher sorption of arsenate versus arsenite on amorphous Al-oxide, effect of ligands. *Environmental Chemistry Letters, 11(3),* 289–294. DOI 10.1007/s10311-013-0405-7.
28. Sahu, R. C., Patel, R., Ray, B. C. (2011). Adsorption of Zn(II) on activated red mud: Neutralized by CO_2. *Desalination, 266(1–3),* 93–97. DOI 10.1016/j.desal.2010.08.007.